

Article

Ceramic Materials in a Ti–C–Co–Ca₃(PO₄)₂–Ag–Mg System Obtained by MA SHS for the Deposition of Biomedical Coatings

Artem Potanin *, Yury Pogozhev, Alexander Novikov and Evgeny Levashov

SHS Research and Education Centre MISIS-ISMAN, National University of Science and Technology, 119049 Moscow, Russia; yspogozhev@mail.ru (Y.P.); avnovikov@inbox.ru (A.N.); levashov@shs.misis.ru (E.L.)

* Correspondence: a.potanin@inbox.ru; Tel.: +7-495-236-3291

Received: 11 August 2017; Accepted: 11 September 2017; Published: 15 September 2017

Abstract: This study aimed to obtain biocompatible ceramic materials in a Ti–C–Co–Ca₃(PO₄)₂–Ag–Mg system by the combustion mode of mechanically activated (MA) reaction mixtures. The influence of the MA time on the reaction ability capability of the mixtures, on their structural and chemical homogeneity, on the combustion parameters and structural-phase conversions in the combustion wave, as well as on the structure and phase composition of the electrode materials has been researched. It was found that the intense treatment of powder mixtures causes plastic deformation of components, the formation of lamellar composite granules, a reduction in the sizes of coherent scattering regions, and also the formation of minor amounts of products. The influence of the activation duration of the ignition temperature and heat release during the combustion of the reaction mixtures was studied. By the method of quenching the combustion front, it was demonstrated that in a combustion wave, chemical transformations occur within the lamellar structures formed during the process of mechanoactivation. It was shown that in the combustion wave, parallel chemical reactions of Ti with C as well as Ti with Co and Ca₃(PO₄)₂ occur, with a Ti–Co-based melt forming the reaction surface. Ceramic electrodes with different contents of Ag and Mg were synthesized by force self-propagating high-temperature synthesis (SHS)-pressing technology using the MA mixtures. The microstructure of the materials consisted of round-shaped grains of nonstoichiometric titanium carbide TiC_x grains, intermetallic matrix (TiCo, TiCo₂, CoTiP), inclusions of Ca and Mg oxides, and grains of the Ag-based solid solution. An increased content of Ag and Mg in the composition of the electrodes, as well as an increased MA duration, leads to an enlargement of the inclusions of the Ag-containing phase size and deterioration in the uniformity of their distribution.

Keywords: self-propagating high-temperature synthesis; mechanical activation; structural-phase transformations; electrode material; biocompatible

1. Introduction

The functionalization of surfaces of metallic implants in order to form a necessary surface topography as well as a sufficient level of mechanical qualities, biocompatibility, and bioactivity [1] is a challenge for modern medical tools. The modification of the chemical composition and surface roughness of metallic implants significantly enhances the implants' osteoconductive and osteoinductive characteristics [2–4]. Antibacterial properties of the coatings prevent the adhesion and growth of bacteria on the surfaces of implants, decreasing the risk of microbial infection when such an implant is integrated with living tissues [5]. The application of multicomponent coatings, in the composition of which each phase or element is responsible for different functional properties, will permit the effective engineering of an implant's surface properties. For example, the presence of titanium carbides and nitrides in the coating ensures the implant's hardness and wear-resistance.

To enhance the mechanical properties of the coatings, one has to introduce a biocompatible metallic component, for example, cobalt, into the coating composition. An addition of a little silver ensures the antibacterial properties of the coating; such additions can also serve as lubricants, thus improving the tribological characteristics of the surface [6]. The presence of calcium-phosphate compounds adds bioactive characteristics to the coating and stimulates the growth of new cells of the osseous tissue on the implant surface [2].

The properties of multicomponent biocompatible electrospark coatings in a Ti–Co–Ca–Ag–Mg–C–P–O system deposited using composite electrodes produced by the self-propagating high-temperature synthesis (SHS) method were investigated in [7]. The optimal content of cobalt binder amounting to 20% was established, at which a sufficient level of the coating's mechanical properties, biocompatibility, and bioactivity are achieved. It was shown that the introduction of Ag and Mg into the coatings' composition ensures the antibacterial effect of the coating against *Escherichia coli* (*E. coli*) and *Staphylococcus aureus* (*S. aureus*) at a level of 98–99% over 24 h. However, these additives have some inhibiting effect on the proliferation and differentiation of the osteoblasts. The latter is related to the presence, besides highly dispersed inclusions of silver sized at 100–200 nm, of large particles up to 1 μm in the coating. When such a multicomponent coating is immersed in physiological liquid, microgalvanic effects that damage the living cells [8] appear between the Ag particles and other more electronegative elements (Ti, Mg, Co, or others) in the composition of the coating. An increased dispersity and homogeneity of the distribution of the silver inclusions will permit us to decrease the galvanic currents and will positively influence their release kinetics by virtue of an increased dissolution rate. Moreover, this must favor an accelerated removal of Ag^+ ions from the organism.

A preliminary mechanical treatment of the reaction mixture in high-energy planetary centrifugal mills (PCMs) and attritors [9,10] is an effective method that permits us to decrease the size of the structural constituents and increase the homogeneity of the component distribution in the SHS electrodes. The application of high mechanical forces on the reaction mixture allows us to:

- mechanically activate (MA) the mixture, thus increasing its reaction ability by virtue of a decrease in the crystallite sizes, and an increase in the reaction surface between the components and an accumulation of the crystalline structure defects. The MA method is widely used in SHS technologies at the stage of preliminary treatment of weakly exothermic and hardly ignitable mixtures for combustion synthesis [11–15];
- obtain lamellar granules or multilayer composite structures with a homogeneous distribution of the elements within the crystallites [16–18];
- evenly distribute little amounts (up to 5 wt. %) of alloying nanosized additives, including ones with a considerable difference in density [19,20];
- activate the solid-phase or liquid-phase sintering process [21–23];
- conduct mechanochemical synthesis in the mill drums [24–26].

That is why optimization of the MA regime is an important technological task. As a result of the processes of structural transformation and energy accumulation in the reaction mixture, the initiation temperature for the SHS process decreases and the rate of the reactions as well as the completeness of the chemical conversions rises [9–11,13].

This work has aimed at continuing research [7,27] into the production of electrode materials for the technology of pulsed electrospark deposition (PED) of biocompatible and bioactive coatings with an antibacterial effect. The main attention has been devoted to an analysis of the influence of the MA on the reaction ability of Ti–C–Co– $\text{Ca}_3(\text{PO}_4)_2$ –Ag–Mg mixtures, on their structural and chemical homogeneity, on the combustion parameters and structural-phase conversions in the combustion wave, as well as on the structure and phase composition of the electrode materials.

2. Materials and Methods

Powders of titanium (99.0% purity, $\sim 30 \mu\text{m}$ in size), technical carbon black (99.9% purity, $\sim 0.2 \mu\text{m}$ in size), cobalt (99.5% purity, $\sim 63 \mu\text{m}$ in size), silver (99.0% purity, $\sim 15 \mu\text{m}$ in size), magnesium (99.0%

purity, ~75 μm in size), and tricalcium phosphate $\beta\text{-Ca}_3(\text{PO}_4)_2$ (97.5% purity, ~15 μm in size) were applied as the initial components of the reaction mixture.

The compositions of the reaction mixtures were calculated from the equation $(70\% - X)(\text{Ti} + 0.5\text{C}) + 20\% \text{Co} + 10\% \text{Ca}_3(\text{PO}_4)_2 + X\% (3\text{Mg} + 2\text{Ag})$, where X is the charge mixture parameter equal to 13% and 24%, which conforms to the Ag and Mg content of 4 and 6 at. % as well as 8 and 12 at. %, respectively, in the composition.

Low-energy mixing was performed in a ball rotating mill (BRM) (MISiS, Moscow, Russia) at the following technological parameters: the working volume of the hard-alloy drum was 3 L, the drum rotational speed was 100 rpm, the ratio of the hard-alloy balls' mass to the charge mixture mass was 6:1, and the mixing time was 8 h [7]. High-energy mixing (mechanical activation) was performed in an Aktivator-2S (OOO Machine-Building Plant "Aktivator", Novosibirsk, Russia) high-speed planetary centrifugal mill (PCM) in inert argon atmosphere (1 atm.) at the following technological parameters: the working volume of the steel drums was 250 cm^3 , the drum rotational speed was 700 rpm (70 g), and the ratio of the steel balls' mass to the charge mixture mass was 15:1.

The heat release in the combustion reaction of the MA mixtures was determined using a BKS-2H (ISMAN, Chernogolovka, Russia) fast combustion calorimeter accurate up to 0.2% in the range of $10^3\text{--}10^4$ J under a constant pressure.

The amount of heat generated during the combustion of the MA mixtures was determined using a high-speed combustion calorimeter, BKS-2H, with a precision of up to 0.2%.

The experiments on determining the mixtures' self-ignition temperature were performed in a reaction chamber in an argon flow at a pressure of 1 atm. Tablets with a relative density of 70%, a diameter of 3 mm, and a thickness of ~1 mm were pressed from the reaction mixture and installed on a graphite substrate into a boron nitride crucible with a diameter of 3 mm. The sample ignition temperature was measured using two W-Re5/20 thermocouples, one of which was installed in the lower butt end of the crucible, and the other one was on the sample's surface. The graphite substrate was heated by passing electric current that transferred the heat to the sample. The ignition temperature was determined by a characteristic sharp bend of the temperature profile curve.

To study the dynamics of the structural transformations in the combustion wave, the method of the stopped combustion front (SCF) by quenching in a copper wedge (with a vertex angle of 5°) [14,28] was applied with subsequent scanning electron microscopy (SEM) and energy-dispersive spectroscopy (EDS) of the characteristic SCF areas using a Hitachi S-3400N (Hitachi, Tokyo, Japan) scanning electron microscope equipped with a NORAN (Hitachi, Tokyo, Japan) energy-dispersive X-ray spectrometer. In order to perform the microstructural research, the SCF sample was embedded into a current-conducting resin. This microscope was also used for analyzing the microstructure of the activated reaction mixtures and compact synthesized samples.

The compact materials were obtained using the force SHS-pressing technology in a "sand" mold, according to the methodology [7,13–15,28]. Synthesized parts were polished, and from their central parts the samples were cut using an electroerosive tool in order to perform the X-ray phase and structural research.

The phase compositions of the reaction mixtures and SHS products were studied by an X-ray diffraction analysis (XRD) using monochromatic CuK_α radiation. The scanning was performed in a step-by-step mode in an angle range of $2\theta = 10 \div 110^\circ$ with a filming step of 0.1° and exposure for 6 s at each point. The obtained spectra were processed using the JCPDS cards.

3. Research Results and Discussion

In order to assess the contribution of the MA to the charge mixture's reaction ability, the morphology and structure state of the Ti–C–Co– $\text{Ca}_3(\text{PO}_4)_2$ –Ag–Mg powder mixtures were studied at $X = 24\%$ after 3–11 min of the MA. The size of the coherent scattering regions (CSRs) as well as the Ti and Ag microstrain (ϵ) values were measured using the Rietveld method [29]. The obtained spectra were processed using a special software package [30]. Table 1 presents the XRD results and

Figure 1 provides the diffraction patterns after a certain time of the MA. It can be seen that as the MA duration rises, the CSR becomes smaller and the ϵ value grows. This evidences an accumulation of defects of the material's crystalline structure and growth of the stored energy. Besides the initial components (amorphous C), the mixtures contain titanium hydride TiH_2 due to the calcium-hydride way of obtaining the Ti powder.

Table 1. Influence of the mechanically activated (MA) duration on the phase composition of the Ti–C–Co– $\text{Ca}_3(\text{PO}_4)_2$ –Ag–Mg mixtures at $X = 24\%$, the coherent scattering region (CSR) size, and the Ti and Ag lattice microstrain values.

Phase	α -Ti (<i>hP2/1</i>)			Ag (<i>cF4/1</i>)			TiH_2	Mg	$\text{Ca}_3(\text{PO}_4)_2$	α -Co	AgMg
	wt. %	CSR, Å	ϵ , %	wt. %	CSR, Å	ϵ , %	(<i>cF12/1</i>)	(<i>hP2/1</i>)	(<i>hR92/2</i>)	(<i>hP2/1</i>)	(<i>cP2/1</i>)
MA Duration, min											
3	39	551 ± 50	0.27 ± 0.03	23	232 ± 30	0.21 ± 0.02	5	7	11	15	–
5	49	420 ± 50	0.27 ± 0.03	19	166 ± 30	0.21 ± 0.02	4	3	9	12	4
6	55	405 ± 50	0.28 ± 0.03	16	166 ± 30	0.25 ± 0.03	4	–	9	11	5
7	56	374 ± 40	0.29 ± 0.03	12	155 ± 20	0.40 ± 0.04	5	–	6	8	13
9	59	366 ± 40	0.30 ± 0.03	11	152 ± 20	0.51 ± 0.05	5	–	5	7	13
10	61	364 ± 40	0.33 ± 0.03	8	142 ± 20	0.57 ± 0.06	4	–	6	3	18
11	Mechanochemical synthesis (Refer to Figure 1c)										

The dependence of the microstrain on the duration of the MA is determined by the mixture components' elastic characteristics. For the Ti and Ag lattices, the CSRs decreased equally (for ~ 1.5), but ϵ accumulated more in the silver. The microstrain of Ag rises 3 times as compared to the initial powder, whereas the one of Ti increases only by 30%.

The MA lasting for 1–4 min does not cause any noticeable changes of the mixture's phase composition. As a result of the intense plastic deformation, the crystallites are ground, which is evidenced by a broadening of the peaks that correspond to the α -Ti, Co, and Ag phases (Figure 1).

AgMg intermetallics form in the powder mixture after 5 min of the MA as a result of recurrent destruction and cold-welding processes [31]. If the MA duration increases, the content of AgMg rises and the content of Ag and Mg decreases. The decrease of the $\text{Ca}_3(\text{PO}_4)_2$ and Co peaks' intensity (Figure 1b) indicates an amorphization and a great degree of grinding of these particles [32]; also, a partial dissolution of Co in the Ti is possible. The maximal solubility of α -Co in α -Ti is ~ 1.5 wt. % [33]. Mechanochemical synthesis takes place in the mill drums after 11 min of the treatment. As a result, titanium carbide forms, and TiCo, TiCo_2 , and TiCoP intermetallics also form (Figure 1c).

Figure 2 presents the microstructures of polished samples of the Ti–C–Co– $\text{Ca}_3(\text{PO}_4)_2$ –Ag–Mg powder mixtures at $X = 24\%$ after the planetary milling and demonstrates the changes in the morphology of the mixtures. The mixture prepared in a BRM is characterized by an uneven distribution of the components (Figure 2a,b). The initial particles do not practically change their shape and sizes when stirred. After 3 min of the MA (Figure 2c), as a result of collisions with the milling bodies, the titanium particles are flattened, ground, and the small particles of the other components— $\text{Ca}_3(\text{PO}_4)_2$, C, Ag, and Mg—are evenly distributed. The cobalt particles do not practically change their size and shape. The 5-min MA (Figure 2d) leads to the formation of elongated titanium layers 2–3 μm thick, and between their boundaries there are interlayers of $\text{Ca}_3(\text{PO}_4)_2$, C, Ag, and Mg. Thus, the specific surface of the particles and their contact surface increases. When the treatment duration rises up to 7 min (Figure 2e), the powder particles fuse, and agglomerates that are composite particles sized at 50–100 μm begin to form. At this duration of the activation, the cobalt particles deform and change their shape, and the titanium interlayers become thinner.

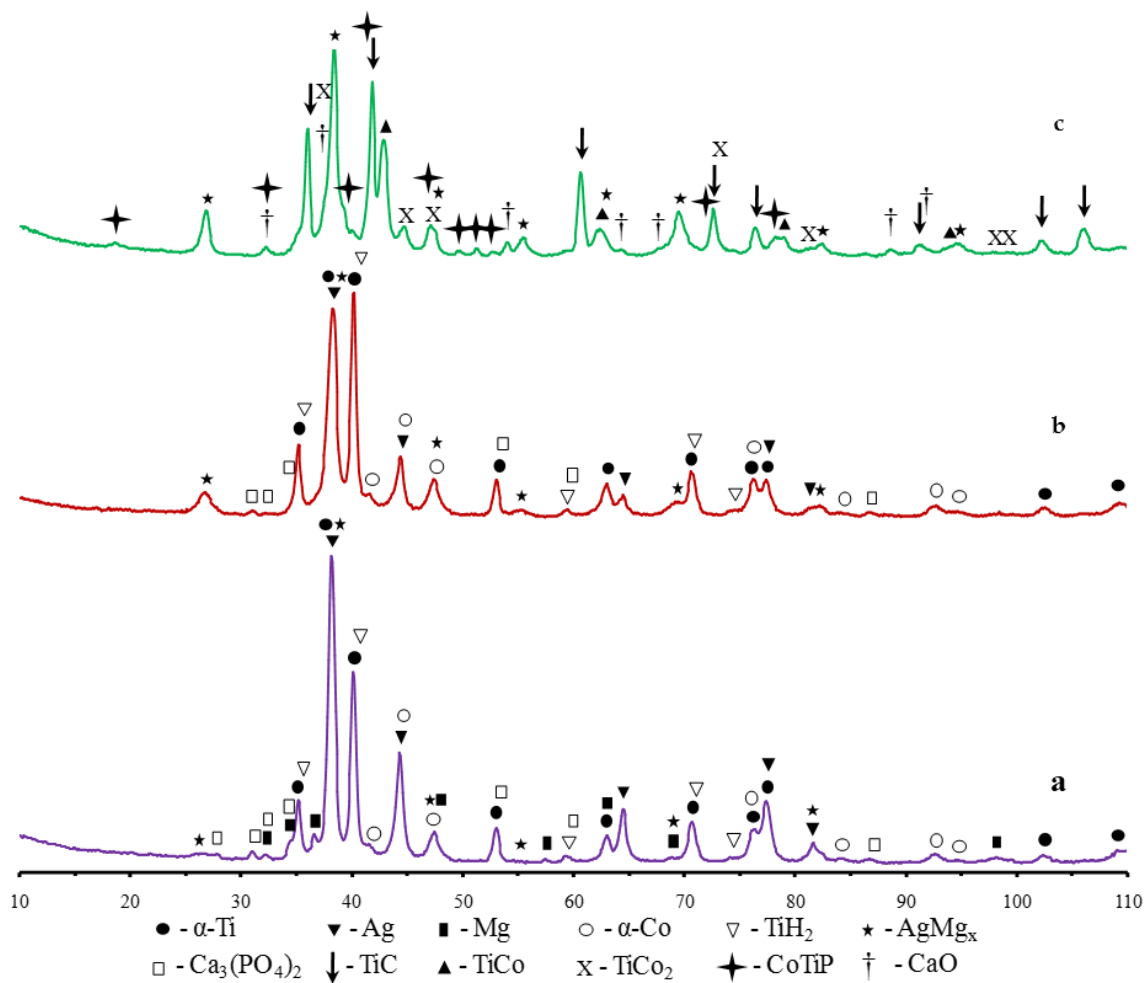


Figure 1. Diffraction patterns of the Ti–C–Co–Ca₃(PO₄)₂–Ag–Mg powder mixtures at X = 24% after the MA lasting for 3 (a), 10 (b), and 11 (c) min.

Figure 2f presents the microstructure of the composite particle after 9 min of the MA. The composite's lamellar structure formed earlier has been destroyed after being exposed to the shear deformation that occurs during the intense mechanical treatment. A homogeneous distribution of the Ca₃(PO₄)₂, C, Ag, and Mg components with titanium and cobalt inclusions with sizes up to 10 μm is observed in the particles. After the mechanochemical synthesis at 11 min of the MA, the structure and morphology of the composite particles does not practically change and consists of grains of the evenly distributed phases of the reaction products (Figure 2g,h). In addition to that, using the EDS method for the structure, Ti particles sized at 6–8 μm have been detected that were not found through the XRD method (Table 1) because of the overlapping diffraction lines of the different phases.

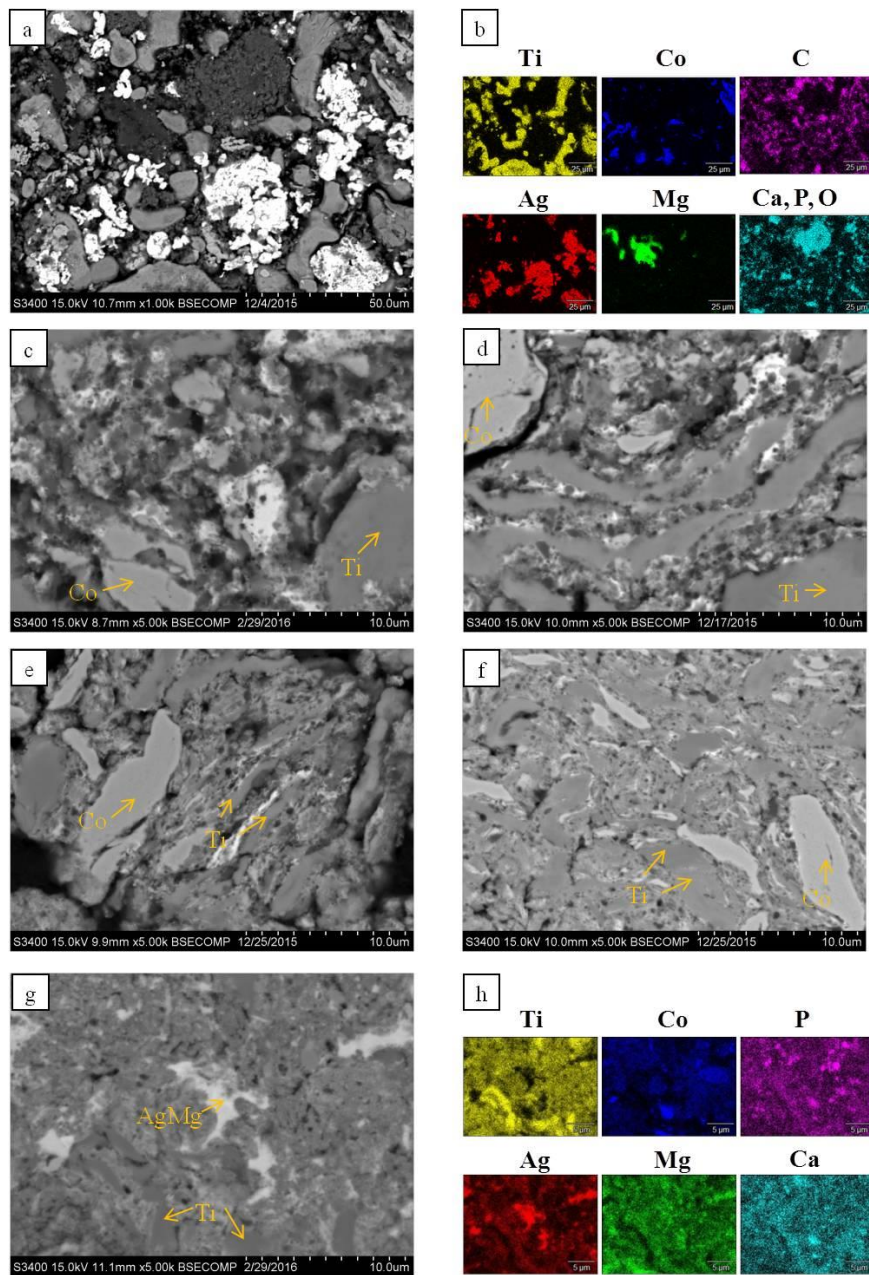


Figure 2. Evolution of the microstructure of the Ti-C-Co-Ca₃(PO₄)₂-Ag-Mg powder mixtures at X = 24% after the ball rotating mill (BRM) (a,b) and MA during 3 (c), 5 (d), 7 (e), 9 (f), and 11 (g,h) min.

Figure 3 presents the results of the calorimetric studies of the Ti-C-Co-Ca₃(PO₄)₂-Ag-Mg powder mixtures at X = 13% and 24% in the form of a chart of the dependence of the generated specific heat on the MA duration. Due to the possibility of several simultaneous reactions with different thermal effects in the multicomponent system during the SHS, the obtained dependencies have complicated profiles that differ from the standard parabolic one [13,14].

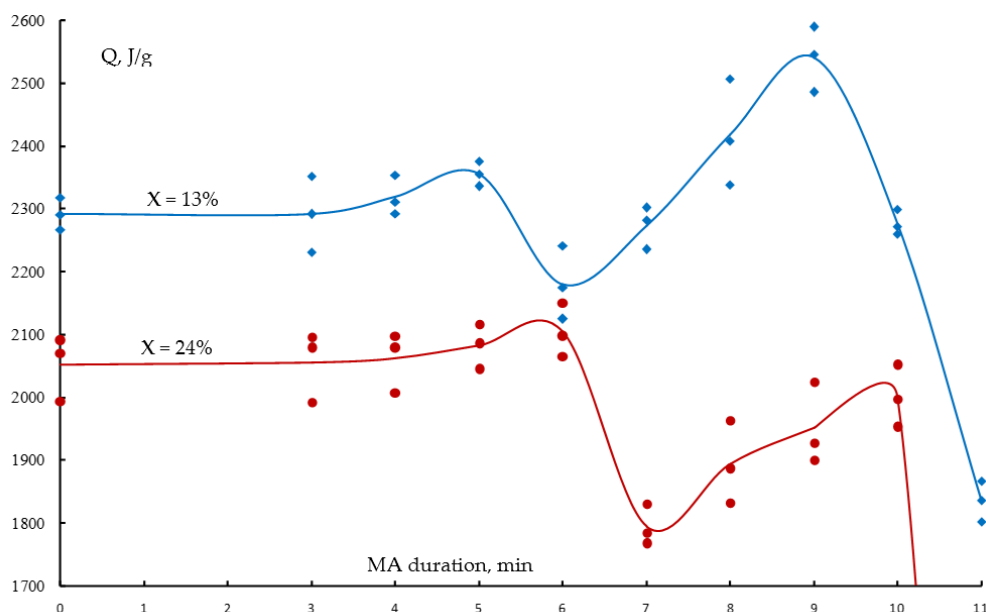


Figure 3. Dependence of the specific heat of combustion on the duration of the MA of the Ti-C-Co-Ca₃(PO₄)₂-Ag-Mg powder mixtures at X = 13% and 24%.

The MA during 5 min (for X = 13%) and 6 min (for X = 24%) generates an insignificant increase in the specific heat released during the combustion of the samples. The further increase of the MA duration leads to a drastic decrease of the heat generation, which is apparently connected with a significant increase of the content of the forming AgMg intermetallics and heat losses necessary for their heating and melting. According to the XRD (Table 1), by the 7th minute of the MA of the composition with X = 24%, the content of AgMg amounts to about 13%, which is ~2.5 times higher than in the mixture treated for 6 min. When the MA lasts for 7 to 10 min, a sharp rise of the specific heat generation from the combustion reaction is observed on the curves. According to the data given in Table 1, when the MA lasts longer, the CSRs of the α -Ti and Ag lattices become smaller and the value ε rises, which increases the mixture's calorific value by virtue of an accumulation of energy on the structural defects and an increase in the reagents' specific surface when forming the composite granules with a lamellar structure. The greatest specific heat generation for the composition with X = 13% is achieved at the MA duration of 9 min. The further mechanical treatment of the mixture initiates chemical reactions and mechanochemical synthesis that take place directly in the mill drums, which results in the formation of the reaction products.

The type of dependence of the specific heat generation for the composition with X = 13% repeats, in general, the course of the curve for the composition with X = 24%, but is characterized by higher heat generation values. This is explained by an increased content of titanium and carbon in the reaction charge mixture, and, consequently, a larger contribution of the exothermic reaction to titanium carbide formation [34].

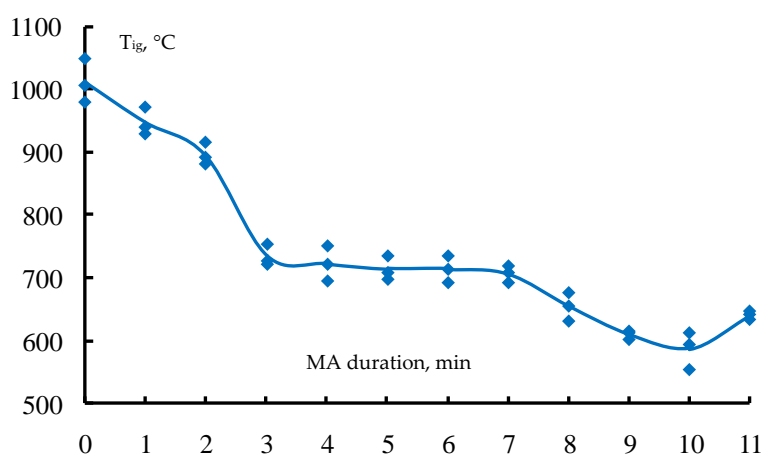
Thus, when the Ti-C-Co-Ca₃(PO₄)₂-Ag-Mg reaction mixture is mechanically activated, competing processes can be marked out: on the one hand, the increase in the reaction surface and accumulation of the energy of the structure defects; and on the other hand, the partial chemical conversion that decreases the system's energetic capabilities.

The composition of combustion products after the combustion of the MA mixture at X = 24% in the high-speed calorimeter is presented in Table 2. Based on the XRD results, it can be concluded that the duration of the reaction mixture treatment does not affect the final phase composition of the synthesized samples. The phase content is almost identical: the difference does not exceed 1–5%. An increasing MA time increased the depth of the combustion reaction conversions, which lead to the disappearance of the reaction intermediates (TiCO₃).

Table 2. Composition of the synthesis products after the combustion of the Ti–C–Co–Ca₃(PO₄)₂–Ag–Mg mixtures at X = 24% in BKS after the MA for 5, 7, and 9 min.

MA Duration, min	5		7		9	
Phase (Pearson Symbol)	wt. %	Lattice Parameter, Å	wt. %	Lattice Parameter, Å	wt. %	Lattice Parameter, Å
TiC (<i>cF8/2</i>)	49	a = 4.311	43	a = 4.309	44	a = 4.310
AgMg _x (<i>cF4/1</i>)	18	a = 4.099	17	a = 4.112	18	a = 4.117
CaO (<i>cF8/2</i>)	6	a = 4.803	7	a = 4.805	6	a = 4.807
TiCo ₂ (<i>cF24/1</i>)	5	a = 6.682	12	a = 6.708	11	a = 6.711
TiCo (<i>cP2/1</i>)	4	a = 2.981	13	a = 2.969	13	a = 2.968
TiCo ₃ (<i>cP4/2</i>)	10	a = 3.618	–	–	–	–
CoTiP (<i>oP12/2</i>)	8	–	8	–	8	–

Figure 4 presents the results of measuring the self-ignition temperature (T_{ig}). The T_{ig} of the non-activated mixture prepared in the BRM was equal to ~ 1010 °C. After 3 min of the MA, the self-ignition temperature decreases by 275 °C. An increase of the MA duration up to 7 min does not practically change the T_{ig} . Within the range of 7–10 min, the self-ignition temperature decreases from 710 °C to 590 °C. A further increase in the activation time leads to the growth of the T_{ig} , which corresponds to the results of the heat generation measurements (Figure 3) within this range, and is explained by the starting chemical conversions that decrease the system's energetic capabilities.

**Figure 4.** Dependence of the self-ignition temperature on the duration of the MA of the Ti–C–Co–Ca₃(PO₄)₂–Ag–Mg powder mixtures at X = 13%.

The combustion wave quenching experiments exemplified by the composition with X = 13% activated for 5 min, with a subsequent energy-dispersive spectroscopy analysis of the characteristic areas of the stopped combustion front, have permitted us to make suppositions about the phase conversion dynamics. The combustion front line is marked in Figure 5a. To the left of this line, there is a pre-heating zone with particles of the initial reagents that have not reacted yet, including the lamellar composite granules formed during the MA (Figure 5b), as well as separately occurring Co and Ti particles. To the right of the combustion front, there is a combustion zone (Figure 5c). The combustion temperature for this composition (~ 1812 °C) measured by the thermocouple permits us to suppose that particles of all of the components except carbon melt in the combustion wave.

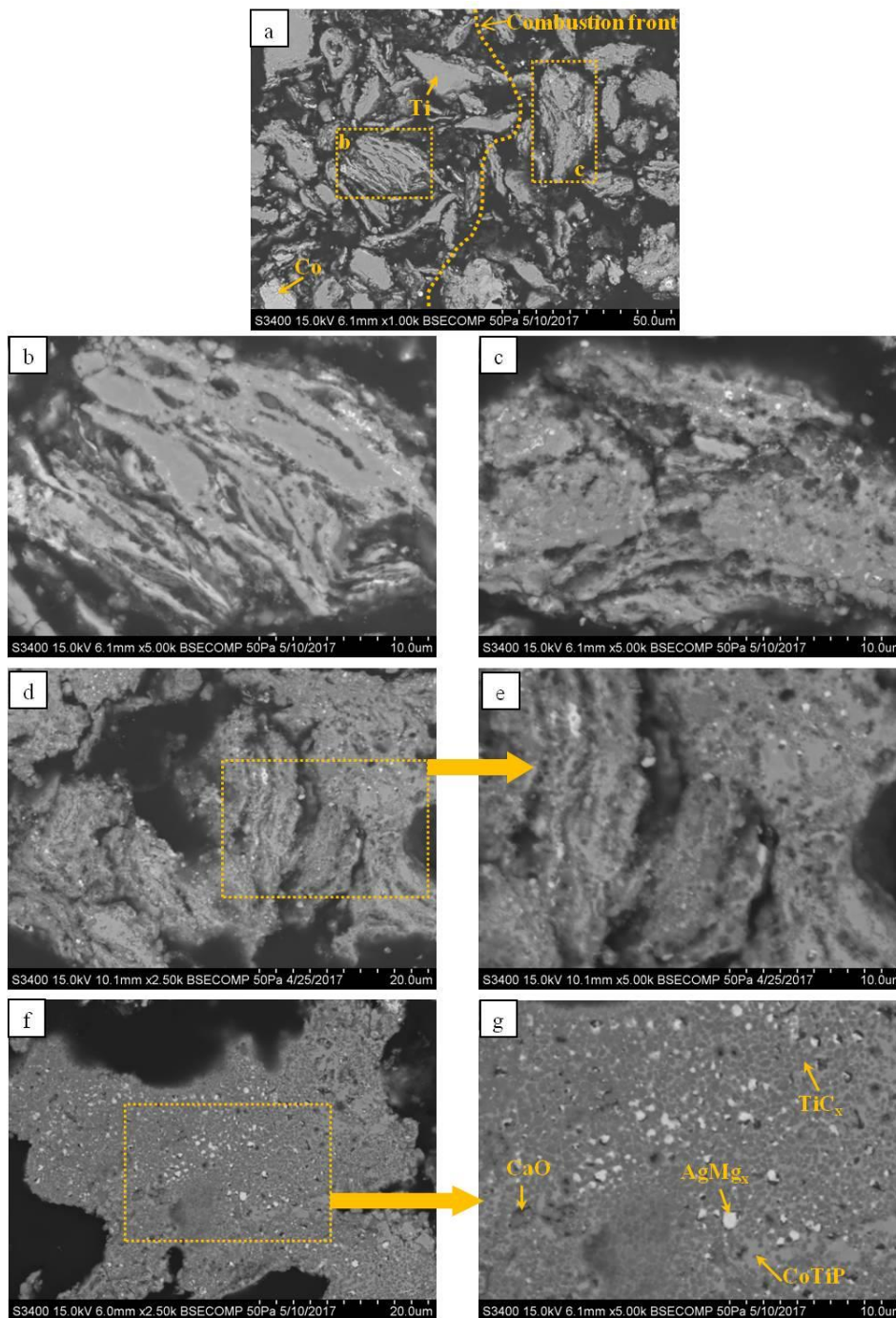


Figure 5. The microstructures of the stopped combustion front (SCF) from the Ti-C-Co-Ca₃(PO₄)₂-Ag-Mg mixture at X = 13% activated for 5 min in various areas of the quenched sample. (a) general view of the sample's SCF; (b) initial charge mixture; (c) combustion zone; (d,e) post-combustion zone; (f,g) final product.

When researching the combustion zone, one can note that the size and shape of the formed melt areas practically coincide with the size and shape of the initial composite lamellar particles (Figure 5b,c). The proximity of the sizes of the reaction mixture powder granules and the quenched area particles in the combustion wave indicates that the chemical conversion—namely, the melting of the component particles, the stirring of the melts, the impregnation of the carbon black surface, and the structurization of the product—takes place within a reaction cell granule. Further, in the post-combustion zone, the

melts fuse (Figure 5d). During detailed research of the post-combustion zone (Figure 5e), small circular grains of titanium carbide TiC_x (size up to 1 μm) have been noted. This phase forms through the known mechanism of reaction diffusion after the formation of a titanium melt and the dissolution of carbon in it [25,34]. Apart from this, one can observe the products of the interaction of titanium and cobalt with tricalcium phosphate: calcium oxide, CaO, as well as CoTiP phosphate phase, distributed over the titanium carbide grain boundaries.

The final product (Figure 5f,g) consists of carbide grains sized up to 1 μm and an interlayer based on a Ti–Co metallic binder, in which phosphorus is dissolved. The carbide grains grow through the coalescence mechanism and diffusion processes in the post-combustion zone as it cools. When the reaction is completing, the concentrations become even within the whole volume of the product, and the composition approximates to equilibrium. The light-colored irregular inclusions sized from 1 to 2 μm are the phase of the silver-based solid solution, in which Mg is dissolved, according to the results of the energy-dispersive spectroscopy analysis.

To obtain compact samples through the force SHS-pressing technology, Ti–C–Co– $Ca_3(PO_4)_2$ –Ag–Mg mixtures of the following compositions were prepared: X = 13% (BRM and MA for 5 and 9 min); X = 24% (MA for 5 min). Table 3 provides the phase composition of the synthesis products. Nonstoichiometric titanium carbide TiC_x is the main phase in all of the samples. The calculated lattice constant of TiC_x in all of the samples is $a = 4.309 \div 4.313 \text{ \AA}$, which corresponds to the stoichiometry of $TiC_{0.6}$ [35]. An addition of Co into the reaction mixture causes its melting in the combustion wave and interaction with a part of the titanium melt. At a temperature of 1325 $^{\circ}C$, TiCo intermetallics with a wide homogeneity area crystallize from the melt. A $TiCo_2$ intermetallic with a cubical crystal structure apparently forms in the post-combustion zone through the peritectic reaction $TiCo + L \rightarrow TiCo_2$ at 1235 $^{\circ}C$ [33].

Table 3. Phase composition of the compact products of the synthesis.

Mixture Composition and Mixing Type	Phase (Pearson Symbol)													
	TiC (cF8/2)		TiCo (cP2/1)		TiCo ₂ (cF24/1)		CoTiP (oP12/2)		AgMg _x (cF4/1)		CaO (cF8/2)		MgO (cF8/2)	
	wt. %	Lattice Parameter, \AA	wt. %	Lattice Parameter, \AA	wt. %	Lattice Parameter, \AA	wt. %	Lattice Parameter, \AA	wt. %	Lattice Parameter, \AA	wt. %	Lattice Parameter, \AA	wt. %	Lattice Parameter, \AA
a (BRM)	61	a = 4.309	20	a = 2.965	–	–	10	a = 6.033 b = 3.557 c = 6.875	7	a = 4.107	2	a = 4.802	–	–
b (5 min of MA)	60	a = 4.313	10	a = 2.969	8	a = 6.714	9	a = 6.033 b = 3.562 c = 6.864	10	a = 4.105	3	a = 4.804	–	–
c (9 min of MA)	50	a = 4.313	–	–	18	a = 6.699	6	–	15	a = 4.104	6	a = 4.801	5	a = 4.213
d (5 min of MA)	44	a = 4.312	20	a = 2.970	7	a = 6.712	10	a = 6.018 b = 3.549 c = 6.877	16	a = 4.117	3	a = 4.804	–	–

Ti–C–Co– $Ca_3(PO_4)_2$ –Ag–Mg at X = 13% (a–c); Ti–C–Co– $Ca_3(PO_4)_2$ –Ag–Mg at X = 24% (d).

In all of the synthesized samples, a ternary compound of complex titanium and cobalt phosphite CoTiP, calcium oxide CaO, and an Ag-based substitution solid solution with a cubical lattice are present. The calculated value of the silver lattice constant equals from 4.104 to 4.117 \AA , which greatly exceeds its standard value ($a = 4.086 \text{ \AA}$), and can be a consequence of the dissolution of Mg in Ag [7]. In the sample obtained from the charge mixture activated for 9 min, besides calcium oxide, there is 5% of MgO. The intense mechanical treatment of the mixture in the high-energy planetary centrifugal mill favors the formation of new reaction surfaces, on which a significant amount of admixture gases is adsorbed while preparing the mixture for the SHS compacting. Since magnesium and calcium have a high affinity for oxygen, during the combustion they actively react and form oxides.

Figure 6 provides the microstructure of the synthesis products. The compact materials consist of circular grains of titanium carbide located in the matrix based on TiCo and $TiCo_2$ intermetallics as well as ternary CoTiP compound. The average size of the carbide grains in the sample synthesized from the BRM mixture (Figure 6a) equals to 2.4 μm . The CaO phase is located in the intergranular areas in the form of faceted crystals. The light-colored irregular inclusions sized from 4 to 6 μm are the phase of the silver-based solid solution, in which 10.5–12.5 at. % of Mg is dissolved, according to the results of the energy-dispersive spectroscopy analysis.

Figure 6b presents the microstructure of the compact sample synthesized from the Ti–C–Co–Ca₃(PO₄)₂–Ag–Mg mixture at X = 13% activated for 5 min. The highly-energetic treatment has reduced the silver inclusions size in the compact product to 1–2 μm and has favored the decrement of TiC_x grains size to 1.4 μm. The compact sample from the mixture mechanically activated for 5 min is characterized by a homogenous structure with an even distribution of the silver-based inclusions, which must ensure a stable speed of removal of Ag⁺ ions from the PED coatings. Apart from this, a diminution of the structural constituents of the material, titanium carbide grains in particular, must increase the intensity of the electrode (anode) dispersion. At an invariable energy of the pulsed discharges, the anode erosion rate will rise owing to a steady flow of small fragments commensurable with the electrode material grains to the substrate (cathode), which results in an enhanced quality of the formed coatings (continuity, thickness, homogeneity) [36–38].

The increased duration of the MA of Ti–C–Co–Ca₃(PO₄)₂–Ag–Mg mixture at X = 13% up to 9 min in order to achieve the maximal heat generation (Figure 3) caused an active emission of gases during the combustion of the reaction mixture, which loosens the sample structure and results in the formation of large pores and cracks (Figure 6c).

The increased content of silver and magnesium (X = 24%) led to the formation of large accumulations of AgMg_x phase (Figure 6d) in the synthesized sample. It should be noted that this compound is the last one to crystallize (in the range of 760–960 °C), and the size of the AgMg_x phase precipitates depends non-linearly on the total volume fraction of silver and magnesium in the alloy (at X = 13%, D_{av}^{AgMg_x} = 1–2 μm; at X = 24%, D_{av}^{AgMg_x} = 10–15 μm). The twofold increase of their content leads to a practically tenfold enlargement of the silver-based solid solution grains. This effect is caused by a coalescence of the AgMg_x melt sites in the post-combustion zone, which additionally deteriorates the homogeneity of the distribution of silver in the sample.

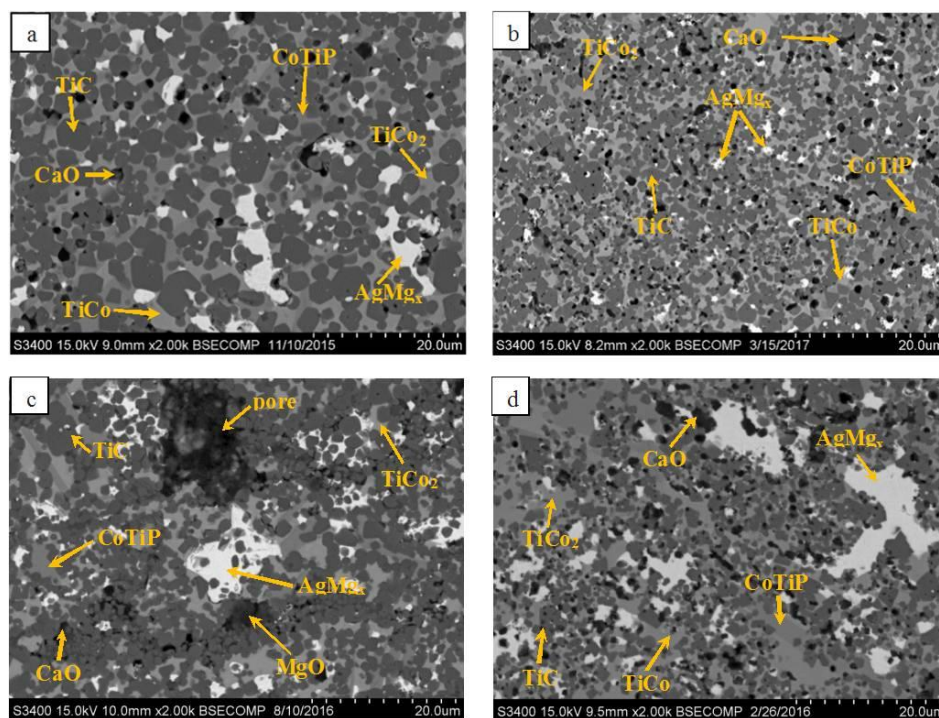


Figure 6. The microstructures of the synthesis compact products from the Ti–C–Co–Ca₃(PO₄)₂–Ag–Mg mixtures composed of: X = 13% (BRM) (a); X = 13% (MA for 5 min) (b); X = 13% (MA for 9 min) (c); X = 24% (MA for 5 min) (d).

Summarizing, we can state that the increased concentration of Ag and Mg is not permissible in the samples. Large grains (globules) of solid (Ag) solution with an inhomogeneous distribution form

because of the strong surface tension and bad wettability of the melt which forms during the synthesis. Moreover, a long MA is also undesirable due to the active emission of gases during the combustion of the reaction mixture, which makes the material's structure less dense.

The optimization of the technological regimes of the force SHS-pressing technology for the Ti–C–Co–Ca₃(PO₄)₂–Ag–Mg reaction mixtures at X = 13% allowed us to produce electrodes with a section of 4 × 4 mm and a length of 40 mm (Figure 7) for the pulsed electrospark deposition of bioactive coatings that have an antibacterial effect. The measured residual porosity of the materials lies within the range of 5–10% optimal for PED. It can be expected that an application of MA to the reaction mixtures will make it possible to enhance the homogeneity of the distribution of alloying additives in the electrodes, which will improve the mechanical and functional properties of the coatings, to which further works will be dedicated.



Figure 7. Pulsed electrospark deposition (PED) electrodes obtained using force self-propagating high-temperature synthesis (SHS)-pressing technology in a Ti–C–Co–Ca₃(PO₄)₂–Ag–Mg system.

4. Conclusions

1. The study has been conducted on the influence of mechanical activation on the structural and phase transformations in the reaction mixtures in a Ti–C–Co–Ca₃(PO₄)₂–Ag–Mg system with the content of Ag amounting to 4 and 8 at. % as well as the content of Mg amounting to 6 and 12 at. % with the MA duration varying from 0 to 11 min. It has been shown that, during the MA, the initial components undergo plastic deformation, there is a formation of lamellar composite granules, a decrease in the coherent scattering regions, a formation of an AgMg intermetallic, and a gradual increase of its content in the mixture.
2. The influence of the MA duration on the ignition temperature and heat generation during the combustion of the reaction mixtures has been investigated. The dependencies are extreme: when the MA duration increases, the starting temperature of the reaction decreases and the reaction mixture's calorific value rises due to an accumulation of macro- and microdefects in the initial powders, and then there is a small increase of the initiation temperature and a decrease of the specific heat generation due to a partial formation of the synthesis products in the mill drum.
3. Ceramic materials with a Co-based metallic binder have been obtained from the MA Ti–C–Co–Ca₃(PO₄)₂–Ag–Mg mixtures using force SHS-pressing technology. The compact ceramics consist of a bound framework of nonstoichiometric TiC_{0.5}–TiC_{0.6}, with phases of intermetallics (TiCo and TiCo₂) which are evenly distributed over the grain boundaries as well as the complex phosphide CoTiP. The introduction of Ag and Mg has resulted in the formation of a silver-based solid solution phase.
4. Electrodes for pulsed electrospark deposition of biocompatible and bioactive coatings, including ones with an antibacterial effect, have been made from the activated Ti–C–Co–Ca₃(PO₄)₂–Ag–Mg reaction mixtures.

Acknowledgments: This work was performed with financial support from the Ministry of Education and Science of the Russian Federation in the frame work of the Increase Competitiveness Program of NUST “MISiS” (No. K2-2016-011) for the part involving the mechanical activation, and from the Russian Foundation for Basic Research (project no. 16-08-00525) for the part involving the study of the samples after SHS-pressing the dense ceramic materials.

Author Contributions: Artem Potanin performed most of the experiments and wrote this manuscript. Yury Pogozhev helped to analyze the experimental data and gave some constructive suggestions. Alexander Novikov helped with some experiments. Evgeny Levashov participated in the results discussion and guided the writing of the article.

Conflicts of Interest: The authors declare no conflict of interest.

References

1. Agarwal, R.; García, A.J. Biomaterial strategies for engineering implants for enhanced osseointegration and bone repair. *Adv. Drug Deliv. Rev.* **2015**, *94*, 53–62. [[CrossRef](#)] [[PubMed](#)]
2. Kelly, M.; Williams, R.; Aojula, A.; O’Neill, J.; Trzińska, Z.; Grover, L.; Scott, R.A.H.; Peacock, A.F.A.; Logan, A.; Stamboulis, A.; et al. Peptide aptamers: Novel coatings for orthopaedic implants. *Mater. Sci. Eng. C* **2015**, *54*, 84–93. [[CrossRef](#)] [[PubMed](#)]
3. Chen, S.H.; Ho, S.C.; Chang, C.H.; Chen, C.C.; Say, W.C. Influence of roughness on in-vivo properties of titanium implant surface and their electrochemical behavior. *Surf. Coat. Technol.* **2016**, *302*, 215–226. [[CrossRef](#)]
4. Shtansky, D.V.; Batenina, I.V.; Yadroitsev, I.A.; Ryashin, N.S.; Kiryukhantsev-Korneev, P.V.; Kudryashov, A.E.; Sheveyko, A.N.; Zhitnyak, I.Y.; Gloushankova, N.A.; Smurov, I.Y.; et al. A new combined approach to metal-ceramic implants with controllable surface topography, chemistry, blind porosity, and wettability. *Surf. Coat. Technol.* **2012**, *208*, 14–23. [[CrossRef](#)]
5. Shtansky, D.V.; Batenina, I.V.; Kiryukhantsev-Korneev, P.V.; Sheveyko, A.N.; Kuptsov, K.A.; Zhitnyak, I.Y.; Anisimova, N.Y.; Gloushankova, N.A. Ag-and Cu-doped multifunctional bioactive nanostructured TiCaPCON films. *Appl. Surf. Sci.* **2013**, *285*, 331–343. [[CrossRef](#)]
6. Sánchez-López, J.C.; Abad, M.D.; Carvalho, I.; Galindo, R.E.; Benito, N.; Ribeiro, S.; Henriques, M.; Cavaleiro, A.; Carvalho, S. Influence of silver content on the tribomechanical behavior on Ag–TiCN bioactive coatings. *Surf. Coat. Technol.* **2012**, *206*, 2192–2198. [[CrossRef](#)]
7. Litovchenko, N.V.; Potanin, A.Y.; Zamulaeva, E.I.; Sukhorukova, I.V.; Pogozhev, Y.S.; Gloushankova, N.A.; Ignatov, S.G.; Levashov, E.A.; Shtansky, D.V. Combustion synthesis of Ti–C–Co–Ca₃(PO₄)₂–Ag–Mg electrodes and their utilization for pulsed electrospark deposition of bioactive coatings having an antibacterial effect. *Surf. Coat. Technol.* **2017**, *309*, 75–85. [[CrossRef](#)]
8. Feng, H.; Wang, G.; Wu, G.; Jin, W.; Wu, H.; Chu, P.K. Plasma and ion-beam modification of metallic biomaterials for improved anti-bacterial properties. *Surf. Coat. Technol.* **2016**, *306*, 140–146. [[CrossRef](#)]
9. Suryanarayana, C. Mechanical alloying and milling. *Prog. Mater. Sci.* **2001**, *46*, 1–184. [[CrossRef](#)]
10. Suryanarayana, C.; Ivanov, E.; Boldyrev, V.V. The science and technology of mechanical alloying. *Mater. Sci. Eng. A* **2001**, *304–306*, 151–158. [[CrossRef](#)]
11. Levashov, E.A.; Kurbatkina, V.V.; Rogachev, A.S.; Kochetov, N.A. Mechanoactivation of SHS system and processes. *Int. J. SHS* **2007**, *16*, 46–50. [[CrossRef](#)]
12. Potanin, A.Y.; Zvyagintseva, N.V.; Pogozhev, Y.S.; Levashov, E.A.; Rupasov, S.I.; Shtansky, D.V.; Kochetov, N.A.; Kovalev, D.Y. Silicon carbide ceramics SHS-produced from mechanoactivated Si–C–B mixtures. *Int. J. SHS* **2015**, *24*, 119–127. [[CrossRef](#)]
13. Eremina, E.N.; Kurbatkina, V.V.; Levashov, E.A.; Rogachev, A.S.; Kochetov, N.A. Obtaining the composite MoB material by means of force SHS compacting with preliminary mechanical activation of Mo–10%B mixture. *Chem. Sustain. Dev.* **2005**, *13*, 197–204.
14. Patsera, E.I.; Kurbatkina, V.V.; Levashov, E.A.; Kochetov, N.A.; Rogachev, A.S.; Umarov, L.M. SHS in mechanically activated Cr–B and Ti–Cr–B blends: Role of gas-transport reactions. *Int. J. SHS* **2012**, *21*, 110–116. [[CrossRef](#)]
15. Patsera, E.I.; Levashov, E.A.; Kurbatkina, V.V.; Kovalev, D.Y. Production of ultra-high temperature carbide (Ta,Zr)C by self-propagating high-temperature synthesis of mechanically activated mixtures. *Ceram. Int.* **2015**, *41*, 8885–8893. [[CrossRef](#)]

16. Loginov, P.A.; Levashov, E.A.; Potanin, A.Y.; Kudryashov, A.E.; Manakova, O.S.; Shvyndina, N.V.; Sukhorukova, I.V. Sintered Ti–Ti₃P–CaO electrodes and their application for pulsed electrospark treatment of titanium. *Ceram. Int.* **2016**, *42*, 7043–7053. [[CrossRef](#)]
17. Rogachev, A.S.; Shkodich, N.F.; Vadchenko, S.G.; Baras, F.; Kovalev, D.Y.; Rouvimov, S.; Nepapushev, A.A.; Mukasyan, A.S. Influence of the high energy ball milling on structure and reactivity of the Ni + Al powder mixture. *J. Alloys Compd.* **2013**, *577*, 600–605. [[CrossRef](#)]
18. Loginov, P.A.; Levashov, E.A.; Kurbatkina, V.V.; Zaitsev, A.A.; Sidorenko, D.A. Evolution of the microstructure of Cu–Fe–Co–Ni powder mixtures upon mechanical alloying. *Powder Technol.* **2015**, *276*, 166–174. [[CrossRef](#)]
19. Yoon, B.; Lee, S.H.; Lee, H. Low-temperature densification of nano Si–C powder containing Al–C additives prepared by high-energy ball-milling. *Ceram. Int.* **2017**, *43*, 12–19. [[CrossRef](#)]
20. Liu, S.; Huang, Z.-L.; Liu, G.; Yang, G.-B. Preparing nano-crystalline rare earth doped WC/Co powder by high energy ball milling. *Int. J. Refract. Met. Hard Mater.* **2006**, *24*, 461–464.
21. Zovas, P.E.; German, R.M.; Hwang, K.S.; Li, C.J. Activated and liquid-phase sintering—progress and problems. *J. Met.* **1983**, *35*, 28–33. [[CrossRef](#)]
22. German, M.R.; Pavan, S.; Seong, J.P. Review: Liquid phase sintering. *J. Mater. Sci.* **2009**, *44*, 1–39. [[CrossRef](#)]
23. Fu, Z.; Koc, R. Processing and characterization of TiB₂–TiNiFeCrCoAl high-entropy alloy composite. *J. Am. Ceram. Soc.* **2017**, *100*, 2803–2813. [[CrossRef](#)]
24. Abbasi, A.R.; Shamanian, M. Synthesis of Mo₅SiB₂ based nanocomposites by mechanical alloying and subsequent heat treatment. *Mater. Sci. Eng. A* **2011**, *528*, 3295–3301. [[CrossRef](#)]
25. Zakeri, M.; Ramezani, M. Synthesis of MoSi₂–TiC nanocomposite powder via mechanical alloying and subsequent annealing. *Ceram. Int.* **2012**, *38*, 1353–1357. [[CrossRef](#)]
26. Suryanarayana, C. Structure and properties of ultrafine-grained MoSi₂ + Si₃N₄ composites synthesized by mechanical alloying. *Mater. Sci. Eng. A* **2008**, *479*, 23–30. [[CrossRef](#)]
27. Sheveyko, A.N.; Manakova, O.S.; Zamulaeva, E.I.; Kudryashov, A.E.; Potanin, A.Y.; Sukhorukova, I.V.; Zhitnyak, I.Y.; Gloushankova, N.A.; Levashov, E.A.; Shtansky, D.V. Structural transformations in TiC–CaO–Ti₃PO_(x)–(Ag₂Ca) electrodes and biocompatible TiCaPCO(N)–(Ag) coatings during pulsed electrospark deposition. *Surf. Coat. Technol.* **2016**, *302*, 327–335. [[CrossRef](#)]
28. Levashov, E.A.; Pogozhev, Y.S.; Potanin, A.Y.; Kochetov, N.A.; Kovalev, D.Y.; Shvyndina, N.V.; Sviridova, T.A. Self-propagating high-temperature synthesis of advanced ceramics in the Mo–Si–B system: Kinetics and mechanism of combustion and structure formation. *Ceram. Int.* **2014**, *40*, 6541–6552. [[CrossRef](#)]
29. Rietveld, H.M. A profile refinement method for nuclear and magnetic structures. *J. Appl. Crystallogr.* **1969**, *2*, 65–71. [[CrossRef](#)]
30. Shelekhov, E.V.; Sviridova, T.A. Programs for X-ray analysis of polycrystals. *Met. Sci. Heat Treat.* **2000**, *42*, 309–313. [[CrossRef](#)]
31. Urretavizcaya, G.; Chávez, A.C.S.; Castro, F.J. Hydrogen absorption and desorption in the Mg–Ag system. *J. Alloys Compd.* **2014**, *611*, 202–209. [[CrossRef](#)]
32. Bae, J.; Ida, Y.; Sekine, K.; Kawano, F.; Hamada, K. Effects of high-energy ball-milling on injectability and strength of β-tricalcium-phosphate cement. *J. Mech. Behav. Biomed. Mater.* **2015**, *47*, 77–86. [[CrossRef](#)] [[PubMed](#)]
33. Ishikawa, K.; Aoki, K.; Himuro, Y.; Ohnuma, I.; Kainuma, R.; Ishida, K. Phase equilibria in the Co–Ti portion of the Co–Al–Ti ternary system. *J. Phase Equilib.* **2001**, *22*, 219–226. [[CrossRef](#)]
34. Potanin, A.Y.; Levashov, E.A.; Pogozhev, Y.S.; Shvyndina, N.V.; Kovalev, D.Y. The features of combustion and structure formation of ceramic materials in the TiC–Ti₃PO_x–CaO system. *Ceram. Int.* **2015**, *41*, 8177–8185. [[CrossRef](#)]
35. Zueva, L.V.; Gusev, A.I. Effect of nonstoichiometry and ordering on the period of the basis structure of cubic titanium carbide. *Phys. Solid State* **1999**, *41*, 1032–1038. [[CrossRef](#)]
36. Levashov, E.A.; Kudryashov, A.E.; Pogozhev, Y.S.; Vakaev, P.V.; Sviridova, T.A.; Zamulaeva, E.I.; Milonich, S.; Todorovich, M. An investigation of the influence of the parameters of pulse discharges on mass transfer, structure, composition, and properties of TiC–NiAl-based electrical spark coatings modified by nanodispersed components. *Russ. J. Non-Ferr. Met.* **2004**, *45*, 32–40.

37. Levashov, E.A.; Vakaev, P.V.; Zamulaeva, E.I.; Kudryashov, A.E.; Pogozhev, Y.S.; Shtansky, D.V.; Voevodin, A.A.; Sanz, A. Nanoparticle dispersion-strengthened coatings and electrode materials for electrospark deposition. *Thin Solid Films* **2006**, *515*, 1161–1165. [[CrossRef](#)]
38. Levashov, E.A.; Kudryashov, A.E.; Pogozhev, Y.S.; Vakaev, P.V.; Zamulaeva, E.I.; Sviridova, T.A. Specific features of formation of nanostructured electrospark protective coatings on the OT4–1 titanium alloy with the use of electrode materials of the TiC-Ti₃AlC₂ system disperse-strengthened by nanoparticles. *Russ. J. Non-Ferr. Met.* **2007**, *48*, 368–378. [[CrossRef](#)]



© 2017 by the authors. Licensee MDPI, Basel, Switzerland. This article is an open access article distributed under the terms and conditions of the Creative Commons Attribution (CC BY) license (<http://creativecommons.org/licenses/by/4.0/>).